energies

MDPI

Article

Experimental Study on Chemiluminescence Properties of Ammonia-Methane Non-Premixed Laminar Flames

Haihang Su [1,2], Yuxuan Wu [2], Jinzhi Yan [1,2] and Liqiao Jiang [1,2,3,*]

[1] College of Energy and Power Engineering, Shenyang University of Chemical Technology, Shenyang 110142, China; suhaihang@outlook.com (H.S.); yanjz@ms.giec.ac.cn (J.Y.)
[2] Guangzhou Institute of Energy Conversion, Chinese Academy of Sciences, Guangzhou 510640, China; cyhd_wyx@163.com
[3] Guangdong Provincial Key Laboratory of Renewable Energy, Guangzhou 510640, China
* Correspondence: jianglq@ms.giec.ac.cn

Abstract: The fundamental investigation on the chemiluminescence characteristics of NH_3-based flames is essential for the development of low-cost, real-time optical diagnostic sensor technologies. In this study, we have experimentally examined the chemiluminescence properties of non-premixed ammonia-methane laminar jet flames under various initial NH_3 blending ratios (X_{NH3} from 0.2 to 1.0 in volume) by conducting the emission spectrum analysis within the 200–800 nm band and capturing the distribution images of key excited radicals. The results revealed that the emission spectra of OH*, CH*, CN*, NH*, and NH_2* were clearly identifiable. As anticipated, the chemiluminescence characteristics of NH_3-CH_4 non-premixed flames were significantly influenced by X_{NH3}; i.e., the overall signal intensity decreased monotonically within the 200–400 nm band but increased within the 400–800 nm band as X_{NH3} increased. The signal intensity characteristics of OH*, CH*, NH*, and NH_2*, indicated by radical images, were consistent with the spectrometer measurements. Particularly, it was found that the intensity ratio of CH*/NH_2* was an ideal marker of initial X_{NH3} in present flames, given their sensitivity with X_{NH3} and relative ease of measurement with the cost-effective sensors designed for invisible wavelengths. Moreover, in the flame front, CH* was located in the oxidant side, while NH_2* was in the fuel side with a broader distribution zone. An increase of X_{NH3} led to greater flame thickness and shifted the peak position of excited radicals far away from the fuel side.

Keywords: chemiluminescence; excited radicals; ammonia-methane ratio; non-premixed flame

check for updates

Academic Editor: Toufik Boushaki

Received: 15 November 2024
Revised: 9 January 2025
Accepted: 14 January 2025
Published: 17 January 2025

Citation: Su, H.; Wu, Y.; Yan, J.; Jiang, L. Experimental Study on Chemiluminescence Properties of Ammonia-Methane Non-Premixed Laminar Flames. *Energies* **2025**, *18*, 402. https://doi.org/10.3390/en18020402

Copyright: © 2025 by the authors. Licensee MDPI, Basel, Switzerland. This article is an open access article distributed under the terms and conditions of the Creative Commons Attribution (CC BY) license (https://creativecommons.org/licenses/by/4.0/).

1. Introduction

Ammonia (NH_3) is a promising hydrogen energy carrier due to its economical storage and transportation in the liquid phase [1]. Recently, the combustion of carbon-free NH_3 fuel for heat or power generation has garnered increasing attention for its ability to reduce carbon emissions [2,3]. However, the combustion diagnostics for NH_3-based fuels remain at an empirical stage and face new challenges. The fundamental investigations on the chemiluminescence characteristics of flames are very important in understanding the combustion process with diverse fuels [4] and for developing sensors for monitoring combustion efficiency, detecting pollutants, and revealing reaction mechanisms. Flame chemiluminescence originates from the spontaneous emission of radiation as active excited radicals transition from a high energy level to a lower one. In general, hydrocarbon flames produce numerous excited radicals, such as OH*, CH*, C_2* [5], etc., whose emission

spectra can reveal the structure, temperature, and concentration distribution of the combustion process. Chemiluminescence-based, non-invasive optical sensors can offer real-time, multi-parameter synchronous measurement capabilities at a low cost [4,6]. To develop high-performance chemiluminescence-based sensors for diagnosing combustion processes with NH_3-based fuels, it is crucial to understand the fundamental chemiluminescence characteristics of NH_3 flames.

The chemiluminescence characteristics of hydrocarbon flames and NH_3 flames exhibit significant differences. Numerous studies have documented the chemiluminescence properties of premixed flames utilizing pure NH_3 and NH_3-blending fuels. For example, Pugh et al. [7] examined the chemiluminescence of NH_3–air and NH_3-H_2–air flames in a fuel-flexible generic swirl burner, employing time-resolved OH*, NH*, and NH_2* chemiluminescence to assess combustion performance. Zhu et al. [8] measured the chemiluminescence spectra in NH_3-CH_4 laminar premixed twin-flames with an NH_3 blending ratio (X_{NH3} in volume) not exceeding 0.8, proposing that CN*/OH* and CN*/NO* intensity ratios could be used to indicate the equivalence ratio and that the NH*/CH* intensity ratio could infer the ammonia fraction under certain conditions. Weng et al. [9] conducted a spatially resolved spectroscopic study on various premixed ammonia–air–oxygen flames stabilized on a laminar flat flame burner by capturing the high-resolution spectra of visible (400–700 nm) chemiluminescent emissions from NO_2* and NH_2*. Their findings indicated that NO_2* dominated in fuel-lean flames, while NH_2* was prevalent in fuel-rich flames. Furthermore, Guiberti et al. [10] developed a machine learning algorithm that was capable of predicting the equivalence ratio and ammonia fraction of premixed ammonia–methane–air flames. They found that the CN*/NO* and NH*/CH* ratios could be utilized to predict the equivalence ratio and ammonia fraction, respectively.

Non-premixed flames are frequently employed in practical combustion devices for safety reasons, specifically to prevent flashback. Although there is a substantial body of research on the chemiluminescence of premixed NH_3-based flames, investigations on the chemiluminescence of non-premixed NH_3-based flames remain limited. In fact, only a few studies have focused on the chemiluminescence of NH_3-based non-premixed flames. For instance, Ku et al. [11] observed the transition from blue to orange colors and an intensified chemiluminescent zone in ammonia–methane non-premixed counter-flow flames with increasing ammonia fractions. Tu et al. [12] compared the chemiluminescence characteristics of non-premixed and premixed NH_3-CH_4–air swirl flames with X_{NH3} less than 0.6. The study indicated that, in premixed combustion, the chemiluminescence intensity ratios of OH*/CH* and CN*/OH* could be the markers of X_{NH3}, but in non-premixed combustion, only NH*/CH* was recommended as the marker of X_{NH3}. Since the responses of chemiluminescence intensity among different excited radicals relative to the changing of X_{NH3} are different between premixed and non-premixed combustion modes, the chemiluminescence characteristics of non-premixed NH_3 flames need more investigations. Because of the inactive combustion attribute of NH_3 [2,3], obtaining stable non-premixed laminar jet flames with pure NH_3 is relatively difficult. The chemiluminescence characteristics of pure NH_3 and stable NH_3-CH_4 non-premixed flames, particularly with high NH_3 blending ratios, are also undiscovered.

In this study, we have investigated the chemiluminescence characteristics of non-premixed NH_3-CH_4 laminar co-flow jet flames by measuring the emission spectra, the chemiluminescence intensity, and the spatial distribution of key excited radicals over a wider range of initial NH_3 blending ratios. The experimental data can be used to validate the chemical reaction mechanisms of chemiluminescence in NH_3-CH_4 fuel flames, as well as to help for developing chemiluminescence-based non-invasive optical sensors in practical ammonia–methane combustion applications.

2. Experimental Methods

2.1. Burner and Flame Cases

In the present experiment, a modified McKenna burner (Holthuis & Associates, Sebastopol, CA, USA) was utilized to generate stable laminar co-flow jet flames for chemiluminescence diagnosis. As depicted in Figure 1, the burner consists of a central tube (inner diameter 4.5 mm) for fuel delivery and a sintered bronze beads plate (diameter 60 mm) for air suppling. To establish stable, pure NH_3 and NH_3-CH_4 non-premixed flames, a stainless-steel plate (diameter 60 mm, height 25 mm) was positioned above the burner exit to stabilize the flames. The distance between the fuel tube exit and the flow-stabilizing plate was adjustable and was set at 23.0 mm for this study. A quartz tube (inner diameter 84 mm, height 200 mm) was attached to the burner to shield the flames from ambient air. To achieve the desired NH_3-CH_4 non-premixed flames with various NH_3 blending ratios, pure NH_3, CH_4, and dehydrated air flows were regulated by mass flow meters, each calibrated by a wet flowmeter prior to the experiment, ensuring an accuracy of greater than $\pm 1\%$. For all flames, the fuel and air velocities were maintained at 60 cm/s and 12 cm/s, respectively. The NH_3 blending ratio (X_{NH3}), representing the volume fraction of NH_3 in the blending fuels, was calculated using the Formula (1). As in the literature [13], the initial mixture strength, ϕ, is defined as the stoichiometry-normalized ratio of the fuel to oxidizer mass fractions at their respective boundaries. Considering the different cross-section areas of fuel and air inlets in the present study, it was $\phi = 0.267$ for pure CH_4/air and $\phi = 0.09965$ for pure NH_3/air non-premixed flames, respectively. Because the air was excessive at ϕ varied from 0.267 to 0.09965, the heat release/chemiluminescence of flames influenced by initial mixture strength could be avoided. In addition, the fixed air and fuel flow rate could keep a stable flow field. All experiments were conducted at atmospheric pressure and an initial temperature of 300 K.

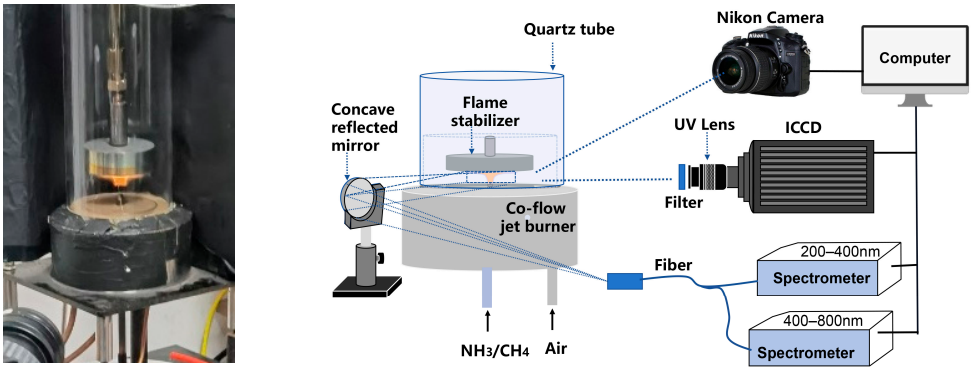


Figure 1. Photo of the burner and the schematic diagraph of optical measurement system.

The NH_3 blending ratio by volume was calculated by

$$X_{NH_3} = \frac{Q_{NH_3}}{Q_{CH_4} + Q_{NH_3}} \quad (1)$$

where Q_{NH_3} is the volume flow rate of NH_3 and Q_{CH_4} is the volume flow rate of CH_4.

2.2. Optical Diagnostics

As shown in Figure 1, the optical diagnostics in this experiment include spectrum measurement and flame imaging. We utilized two portable spectrometers to capture the chemiluminescence spectra of the flames. The light signal collection region was positioned between the flame stabilizer and burner exit. The emission light from the entire flame was focused by using a UV-enhanced concave reflective mirror (25 mm in diameter, 50 mm focal

length) and directed into a Y-type fiber splitter (Ocean Optics, Ostfildern, Germany) with two outputs. The diameter of the optical fiber probe is 3.0 mm. The outputs were linked to two portable spectrometers (Ocean Optics HR4000), each covering a detection range of 200–400 nm and 400–800 nm, respectively, allowing for a combined spectra acquisition from 200 to 800 nm. The spectral resolution of 0.1 nm is adequate for resolving the broad band structures. The flame chemiluminescence within the ultraviolet, visible, and near-infrared bands was measured accordingly. To achieve optimal signal intensity, the integration time was set to 8 s for the 200–400 nm range and 2 s for the 400–800 nm range. The raw spectra were corrected and calibrated using standard light sources (Thorlabs SLS204 and SLS201 Lamps, Newton, NJ, USA) spanning from 200 to 800 nm. Every separated peak signal had a baseline signal (the background signal) adjacent to its excited wavelength. During data processing, due to the lower signal-to-noise ratio, the spectral data within the wavelength range of 200–400 nm were smoothly fitting after subtracting the background signals.

A digital camera (Nikon D750 with a Nikon 180 mm lens, Tokyo, Japan) was employed to directly capture the visible light (RGB) images of flames without a filter. The camera settings were an exposure time of 1/8 s and an aperture of f/5.6. Based on the spectrometer readings, an sCMOS camera (Dhyana 95V2, Tucsen Inc., Fuzhou, China) equipped with an achromatic UV lens (105 mm, f/4.5) and various narrow bandpass filters was used to image key excited radicals. The filters had center wavelengths of 307, 337, 430, and 630 nm, each with a $\pm$10 nm bandwidth. The sCMOS camera provided a resolution of 2048 $\times$ 2048 pixels, and an average of 50 images was taken for each flame case. For the images, the background signals from flame chemiluminescence are difficult to subtract, requiring at least two calibrated cameras to image the different passband filtered flames synchronously. In the present study, the background signals from ambient could be subtracted by averaging the pixel values of the 50 $\times$ 50 pixels in the flame-free region of each measured image.

The distributions of active excited radicals at the flame front are determined by reconstructing the chemiluminescence intensity field by Abel inverse transformation, as detailed in our previous study [14]. Abel's integral equation has been widely used in studies on axisymmetric flames. We utilized the onion-peeling method to calculate the excited radical distributions. A MATLAB(R2023a) deconvolution program was established and employed to reconstruct the axisymmetric non-premixed jet flames. The draw images of radicals were recorded by the sCMOS camera at 2028 $\times$ 2048 pixels^2. After image pre-processing, such as cropping, matching, background signal subtracting, data smoothing, and intensity normalizing, the effective flame signal data could be obtained and then utilized as the integral signal for Abel's transform directly. The size of the grid used to reconstruct the ROI (Region of Interest) of flames was 690 $\times$ 1370 (height $\times$ width) pixels^2. There exists the ill-conditioned set of the matrix constructed by the onion-peeling method, namely, even a slight noise in the project signal will cause the solution incorrect. The onion-peeling method combined with a Tikhonov regularization is less sensitive to measurement errors [15]. Here, we used the interpolation and average data smoothing method to reduce the errors, the reconstruction results show it agrees well with the flame profiles.

3. Results and Discussions

3.1. Flame Morphology

The direct recordings of non-premixed flames by the digital camera (DC) are presented in Figure 2. Throughout all tested flame cases, the fuel flow rate and the corresponding air flow rate remained constant. The flame stabilizer enabled the achievement of higher NH_3 blending ratios in NH_3-CH_4 and even pure NH_3 non-premixed flames. These impinging jet flames exhibited a yellow/orange color and were approximately symmetrical. As the X_{NH3} increased, the flame became unstable due to the lower burning velocity of NH_3.

Consequently, the flame gradually moved farther away from the burner exit, and the yellow/orange flame became brighter. Furthermore, at X_{NH3} = 0.2 and 0.4, a thin, faint purple/blue zone appeared near the outer flame profile, primarily due to the enhanced emission of excited radicals in the UV band when more methane is burning. To prevent the interference from the thermal radiation of high-temperature soot particles, X_{NH3} was set to no less than 0.2 in the current experiment because soot particles would have generated in the top zone of flames with X_{NH3} < 0.2 in NH_3-CH_4 and pure methane non-premixed flames.

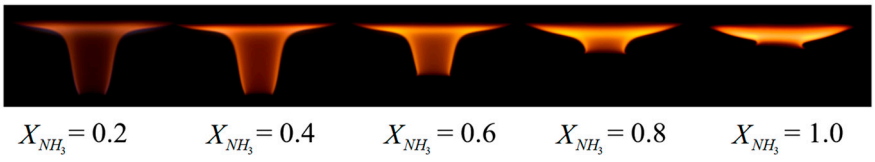


Figure 2. Photographs of non-premixed NH_3-CH_4 flames at NH_3 blending ratio X_{NH3} = 0.2, 0.4, 0.6, 0.8 and 1.0.

3.2. Chemiluminescence Spectrum

The data in Figure 3 show the chemiluminescence spectra of NH_3-CH_4 non-premixed flames. The measured chemiluminescence intensity, integrated within a fixed detection zone, represents a global value for the flames. The spectra are complex, showing numerous spectral transition lines against a broadband background signal. The characteristic emission wavelengths of key excited radicals are indicated in Figure 4, both with and without background signals removed at X_{NH3} = 0.4. Many intensity peaks were observed across the Ultraviolet (UV) to Near Infrared (NIR) spectrum, including wavelengths near 310 nm, 335 nm, 360 nm, 390 nm, 430 nm, 495 nm, 540 nm, 570 nm, 600 nm, 630 nm, 656 nm, and 735 nm. These peak signals, marking important excited radicals, have been documented in the literature [8–10,12,16,17] with NH_3-CH_4–air premixed and non-premixed NH_3-CH_4 flames. Specifically, the OH* emission near 310 nm is attributed to the OH A-X transition, the NH* emission at 336 nm to the NH A-X transition, the CN* emissions at 358 nm (CN A-X) and 390 nm (CN B-X) transitions, the CH* emissions near 430 nm (CH A-X) and 390 nm (CH B-X) transitions, the NO_2* emission near 600 nm to the NO_2 A-X transition, and the NH_2* emission near 630 nm to the NH_2 A-X transition. The data in Figure 3 confirm the presence of these excited radicals in NH_3-CH_4 non-premixed flames. Notably, the emission spectra within the 500–800 nm range are intricate due to various transitions of polyatomic excited radicals, such as NO_2*, NH_2*, and H_2O*. Moreover, the enhanced radiation in the NIR band might be due to water vapor emission, with a particularly intense spectral feature around 735 nm.

The NH_3 blending ratio significantly influences the chemiluminescence spectra of NH_3-CH_4 non-premixed flames. In the 200–400 nm wavelength range, the overall chemiluminescence intensity decreased monotonically with increasing X_{NH3}, particularly for OH*, CH*, and CN* radicals, which are closely related to carbon-based element reactions. Conversely, in the 400–800 nm range, the overall signal intensity increased with the increase of X_{NH3} due to radicals like NH_2* and NO_2* being closely related to nitrogen-based element reactions. However, the C_2* emission signals at 470 nm, 516 nm, and 550 nm were weak, especially in flames with higher X_{NH3}. Overall, the measured signal intensity was weaker in the UV band but relatively stronger in the visible and NIR bands. Therefore, more sensitive sensors are required in the UV band compared to the visible band for developing chemiluminescence-based diagnostic devices for NH_3-based flames.

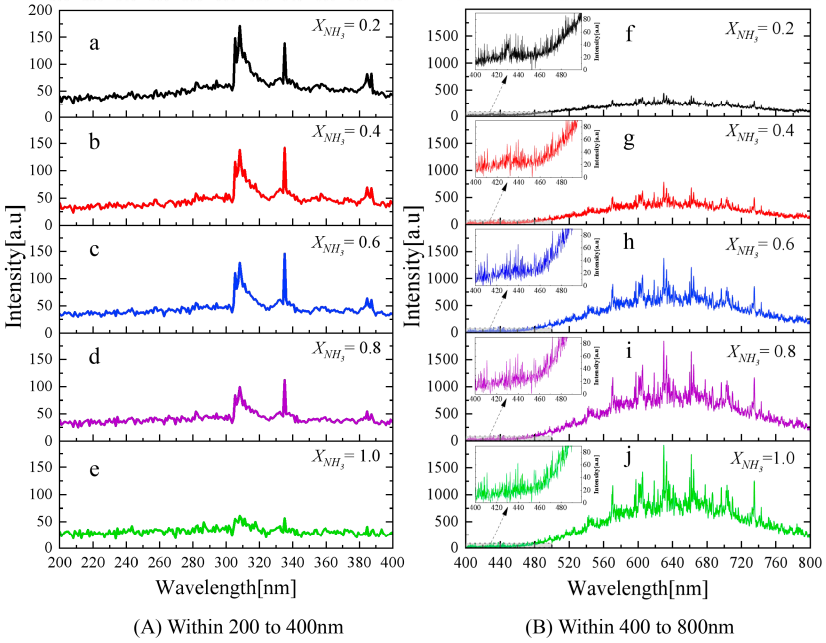


Figure 3. Chemiluminescence spectra (**a**–**j**) of NH_3-CH_4 non-premixed flames at different NH_3 blending ratios (**A**: 200–400 nm; **B**: 400–800 nm). (**a**–**e**) show the Chemiluminescence spectra in UV band (200–400 nm) at various NH_3 blending ratios (X_{NH3} = 0.2, 0.4, 0.6, 0.8 and 1.0), respectively. Subfigures (**f**–**j**) show the Chemiluminescence spectra in Visible band (400–800 nm) at various NH_3 blending ratios (X_{NH3} = 0.2, 0.4, 0.6, 0.8 and 1.0), respectively.

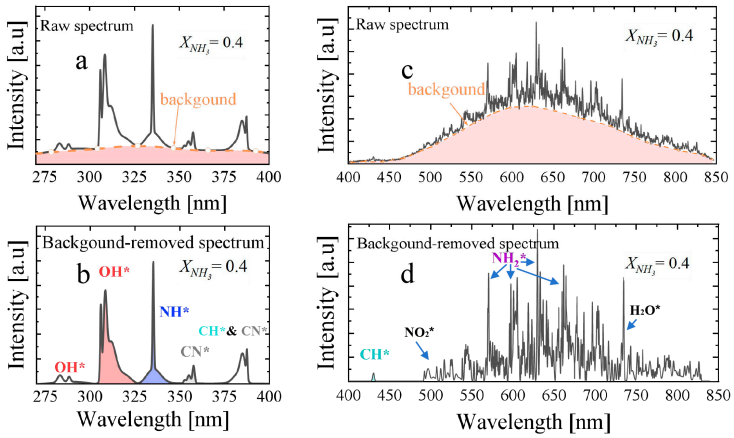


Figure 4. Characteristic emission wavelengths of key excited radicals in the flames, marked both with (**a**,**c**) and without background removal (**b**,**d**) at X_{NH3} = 0.4.

Observations also indicate that the background signal intensity was weakened in the UV band with increasing X_{NH3}, but it was enhanced in the visible and NIR bands. The thermal radiation signal from non-soot flames in the UV band is typically negligible when the flame temperature remains below 2500 K, as reported by Guethe [6]. Consequently, background signals are predominantly due to the chemiluminescence of carbon-based polyatomic molecules, including HCO*, CO_2*, and CH_2O*, within a wavelength range not exceeding 450 nm, as described by Kopp et al. [18] and Samaniego et al. [19]. In hydrocarbon fuel flames, CO_2* emissions, coming from the reaction CO + O + M → CO_2* + M, constitute the primary background signal in the 340–600 nm range. Thus, in flames with increasing X_{NH3}, the reduced production of CO_2, HCO, and CH_2O led to a decrease of background intensity. Between 450 and 800 nm, the background signals were likely emanating from the chemiluminescence of nitrogen-based polyatomic molecules. The mechanism behind the

continuous emission from these molecules remains unknown. Furthermore, an increase in X_{NH3} led to a higher production of nitrogen-based polyatomic molecules, which in turn corresponded to an increase of the background signals.

3.3. Images of OH/NH*/CH*/NH_2* Radicals*

Spectrum analysis can effectively identify the emission wavelengths of excited radicals but cannot reveal their spatial distribution in flames. Instead, the spatial distribution of these radicals can be measured by the sCMOS images with narrow bandpass filters. According to the characteristic emission spectra, in the ultraviolet band, the center wavelengths at 307 nm and 336 nm were chosen for detecting OH* and NH* emissions, respectively. Additionally, the center wavelengths at 430 nm and 630 nm were selected for detecting CH* and NH_2* emissions, respectively. It should be noted that adding a filter slightly alters the focal plane of the sCMOS imaging, particularly with the OH* filter. Therefore, we have calibrated the imaging process for each filter to account for these changes.

The data in Figure 5 display the spatial distribution images of OH*, NH*, CH*, and NH_2* radicals in NH_3-CH_4 non-premixed flames. The chemiluminescence intensity values of each excited radical have been self-normalized for comparison. Similar to the images captured by the digital camera, these images exhibit good symmetry, and the overall distribution characteristics of all radicals appear distinct from one another. It is evident that the signal intensity distribution of these excited radicals is highly sensitive to the NH_3 blending ratio. Generally, for OH*, NH*, and CH* radicals, the signal intensity monotonically decreases as X_{NH3} increases. Notably, the OH* intensity declined the most rapidly, showing a faint light signal at X_{NH3} = 1.0. Additionally, the highest signal intensity values for these radicals were observed at the bottom and top zones of flames, respectively. In contrast, only the NH_2* intensity noticeably strengthened with an increase of X_{NH3} due to the NH_2 radical being primarily generated by nitrogen-based reactions [20].

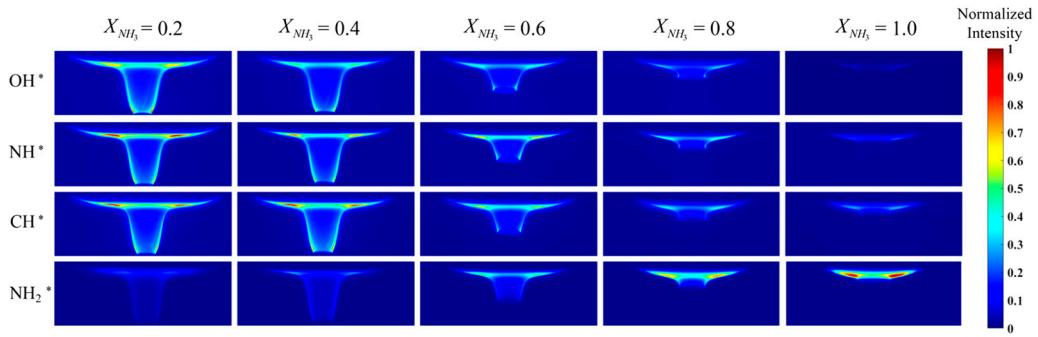


Figure 5. Images of OH*, NH*, CH* and NH_2* radicals in NH_3-CH_4 non-premixed flames.

3.4. Chemiluminescence Intensity Ratios

The overall chemiluminescence signal intensity of various radicals in flames is a crucial parameter for designing chemiluminescence-based sensors. The sCMOS camera, with its higher spatial resolution and better signal intensification effect compared to portable spectrometers, makes it well-suited for quantitatively comparing the chemiluminescence characteristics of NH_3-CH_4 non-premixed flames. The trend shown in Figure 6 illustrates the total signal intensity of each radical in relation to X_{NH3}. Overall, the data in Figure 6 show that as X_{NH3} increased, the total signal intensities of OH*, NH*, and CH* radicals decreased monotonically, while the trend for the NH_2* signal was the opposite.

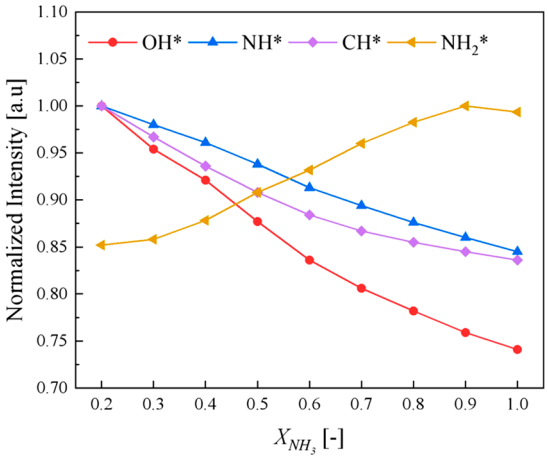


Figure 6. Chemiluminescence intensity of excited radicals as a function of NH_3 blending ratios.

For the OH* radical, a decline in both signal intensity and distribution area was observed, with the signal intensity decreasing the most rapidly as X_{NH3} increased. Previous studies, such as that by García-Armingol et al. [21], have noted that OH* emission is more pronounced in hydrocarbon flames than in hydrogen-enriched premixed flames. This suggests that, in NH_3-CH_4 non-premixed flames, OH* radicals primarily originated from CH species reactions rather than from H species reactions. For the NH_2* radical, the total signal intensity of NH_2* is influenced by a balance between peak signal intensity and the distribution area of the radical. Despite a reduction in the distribution area, the strong peak intensity of NH_2* was dominant, leading to an overall increasing trend in total intensity as X_{NH3} increased. Furthermore, the signal intensity trends of OH* and CH* radicals in relation to NH_3 blending ratios have been observed to be similar in non-premixed NH_3-CH_4 swirl flames [12], but this trend is reverse in premixed flames [8]. This indicates that the effects of NH_3 blending ratios on the intensities of OH* and CH* excited radicals in premixed flames are not applicable to the NH_3-CH_4 non-premixed flames.

The chemiluminescence intensity of a single excited radical is influenced by both the absolute intensity and the flame-front volume. Consequently, this intensity is not suitable for directly marking the NH_3-CH_4 blending ratio in non-premixed flames, especially when the input power is varied. Otherwise, the ratio of chemiluminescence intensities from two different excited radicals can mitigate the impact of varying flame-front volume. With synchronous detection, this approach can fulfill the sensor requirements for detecting the NH_3-CH_4 blending ratio in flames. The data in Figure 7 display how the intensity ratios of four radical pairs in stable flames changed with X_{NH3}. In the figure, every radical as the reference intensity has been compared in turn, although some plots are the same radical pairs. It is evident that all the intensity ratios are very sensitive and decreased monotonically with the increase of X_{NH3} based on NH_2*. Among them, OH*/NH_2* is the most sensitive, then CH*/NH_2* and OH*/NH_2*. Similarly, the OH*/CH* and OH*/NH* pairs are sensitive to X_{NH3}, while the NH*/CH* pairs are less sensitive. In general, the measurement of OH* emissions in the UV band are not cost-efficient for optical detection equipment in industrial applications. Additionally, the CH* radical comes from CH_4 oxidation reactions and NH_2^* from NH_3 fuel. Thereby, the CH*/NH_2* pairs, which can more directly indicate the fuel blending ratio, were recommended as the markers of X_{NH3} in NH_3-CH_4 non-premixed flames. The chemiluminescence of CH*/NH_2* pairs can be efficiently measured by economical visible band photoelectric sensors.

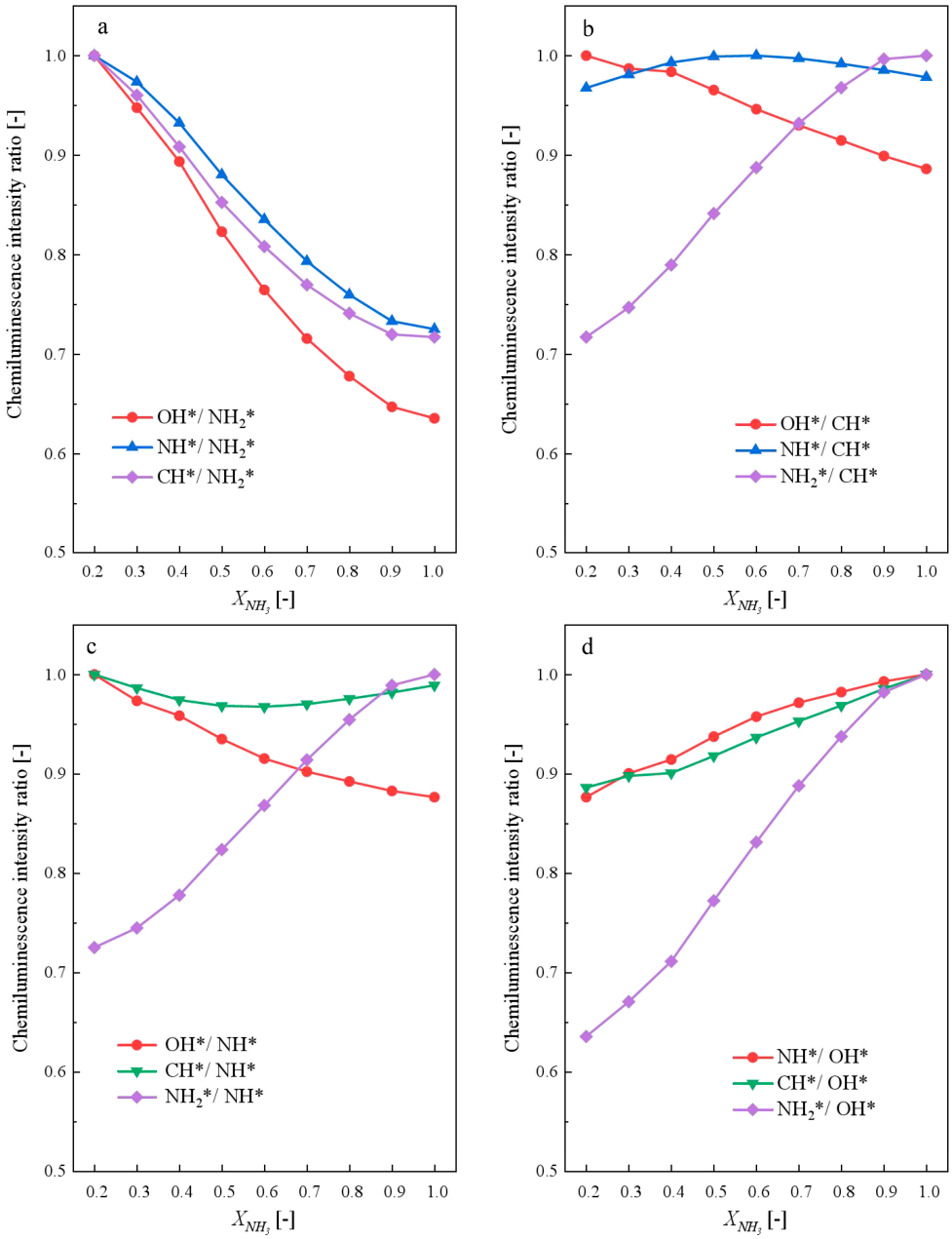


Figure 7. Chemiluminescence intensity ratios of excited radicals as a function of NH_3 blending ratios in NH_3-CH_4 non-premixed flames (**a**–**d**). (**a**–**d**) show the ratio relationship of four radicals based on NH_2*, CH*, NH* and OH*, respectively.

3.5. Radical Distribution in Flamefront

To understand the formation mechanism of key excited radicals in flames, it is essential to determine their distribution in the flame front. By applying Abel inverse transformation to the integrated chemiluminescence intensity images of these excited radicals, we can obtain their distributions. The data in Figure 8 illustrate the distribution of OH*, NH*, CH*, and NH_2* radicals in the flame front at various values of X_{NH3}. It is shown that the strong intensity zone for all radicals was near the base of flames, with the NH_2* radical distribution showing the broadest zone. The distribution of excited radicals along the normal direction of the flame front can be plotted, as depicted in Figure 9 at X_{NH3} = 0.8 and 0.2. There, the chosen position of the flame front for keeping a pure non-premixed flame reaction zone is nearly 1/3 of the flame's length away from the flame root. Overall, it was observed that the chemiluminescence zone enlarged with an increase of X_{NH3}. The enlarged flame front

thickness demonstrates the slower burning velocity effect of increasing X_{NH3} on flame structure. NH_2* was primarily localized in the fuel side zone, followed by NH*, while OH* and CH* occurred in the oxidant side zone. The distance between the NH_2* and OH* distribution curves increases as the X_{NH3} increases. This trend aligns with observations in NH_3-H_2 non-premixed flames by Issayev et al. [22]. Furthermore, a second peak value in the profiles of OH*, CN*, and CH* was observed at X_{NH3} = 0.2, which primarily originated from the outer weak double flame front due to the CH_4 oxidation reaction.

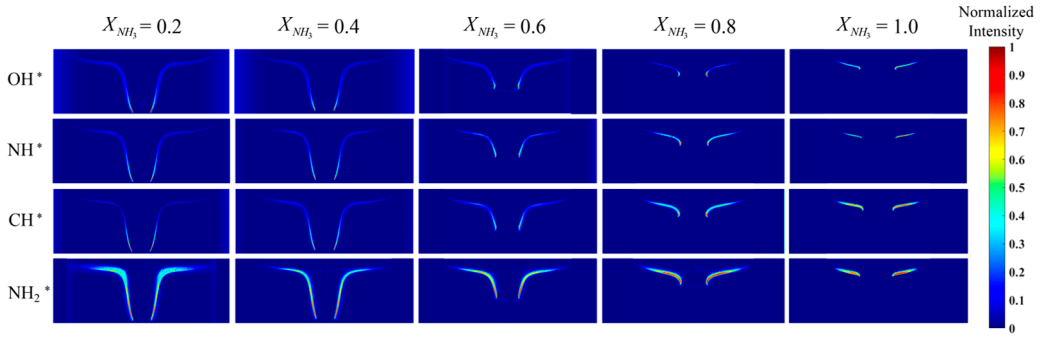


Figure 8. Abel inverse transformation images of excited radicals in NH_3-CH_4 non-premixed flames.

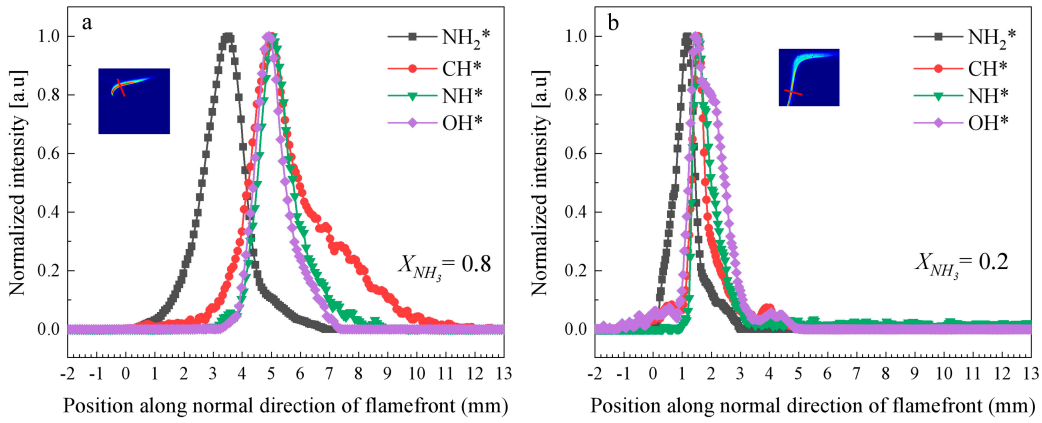


Figure 9. Distribution of excited radicals in flame fronts along normal direction (**a**,**b**). (**a**) shows the distributions of four excited radicals (NH_2*, CH*, NH* and OH*) in flamefront at X_{NH3} = 0.8 NH_3-CH_4 non-premixed flames. (**b**) shows the distributions of four excited radicals (NH_2*, CH*, NH* and OH*) in flamefront at X_{NH3} = 0.2 NH_3-CH_4 non-premixed flames.

The relative positions of excited radicals in the flame front are intimately connected to the reaction mechanisms of NH_3-CH_4 oxidation reactions [23–26]. For NH_3 fuel flames, the primary combustion pathways are $NH_3 \rightarrow NH_2 \rightarrow NH$ and $NH_3 \rightarrow NH_2 \rightarrow HNO \rightarrow NO$. The oxidation pathways for CH_4 are mainly $CH_4 \rightarrow CH_3 \rightarrow CH_2 \rightarrow CH$ and $CH_4 \rightarrow CH_3 \rightarrow CH_2O \rightarrow HCO$. In NH_3-CH_4 flames, the oxidation process of NH_3 and CH_4 mixtures shares a common radical pool for chain reactions, including species such as H, OH, and O. The chemiluminescence reaction kinetics of typical excited radicals in hydrocarbon fuel flames have been well reviewed in previous studies [27,28].

Two significant reactions for forming OH* in pure hydrogen and hydrocarbon flames are

$$H + O + M \rightarrow OH^* + M \quad (2)$$

$$CH + O_2 \rightarrow OH^* + CO \quad (3)$$

For CH*, the three primary formation reactions are

$$C_2 + OH \rightarrow CH^* + CO_2 \quad (4)$$

$$C_2H + O_2 \rightarrow CH^* + CO_2 \quad (5)$$

$$C_2H + O \rightarrow CH^* + CO \quad (6)$$

In the case of pure NH_3 combustion, the simplified reaction path shows that NH_3 first reacts with OH, O, and H to form NH_2. NH_2* chemiluminescence is suggested to originate from the ammonia α band attributed to NH_2 radicals [29–31].

For NH*, it is formed from its precursor NH_2 through the two reactions

$$NH_2 + OH \rightarrow NH^* + H_2O \quad (7)$$

$$NH_2 + H \rightarrow NH^* + H_2 \quad (8)$$

With an increase of the ammonia blending ratio, there is a decrease in fuel reactivity and a subsequent slowdown in reaction rate, which results in the peak position of excited radical moving further from the fuel side, as shown in Figure 10. Notably, the peak position of NH_2* is closer to the fuel side, whereas the peak position of CH* is near the oxidizer side. The peak position of NH* is between these two extremes. The distribution of radicals such as OH* and CH* in the outside of flame front suggests that the oxidation of CH_4 likely precedes that of NH_3 in a non-premixed pattern.

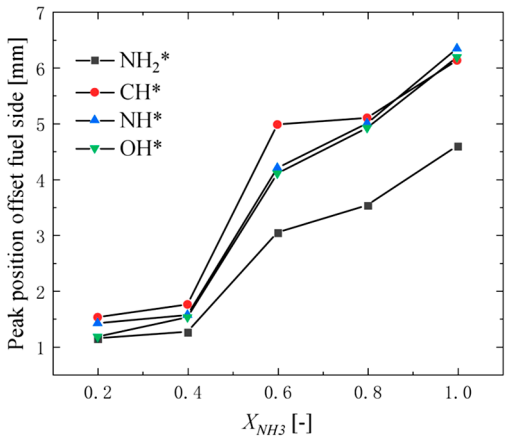


Figure 10. Peak value positions of excited radicals in the flame front of NH_3-CH_4 non-premixed flames as a function of NH_3 blending ratios.

4. Conclusions

Based on spectrum detection by the spectrometer and sCMOS imaging with narrow bandpass filters, the chemiluminescence characteristics of key excited radials in ammonia–methane non-premixed laminar jet flames have been investigated in this experiment. The following results were obtained:

(1) The chemiluminescence spectra of OH*, CN*, CH*, NH*, NH_2*, and NO_2* in non-premixed NH_3-CH_4 flames were identified. Both spectrometer detection and sCMOS images showed that the effect of the ammonia blending ratio (X_{NH3}) on the signal intensity and distribution of these excited radicals was significant: When X_{NH3} varies from 0.2 to 1.0, the chemiluminescence signal intensity of NH*, OH*, and CH* radicals decreases monotonically, but the signal intensity of NH_2* radicals increases monotonically.

(2) The intensity ratios of OH*/NH_2*, CH*/NH_2*, NH*/NH_2*, and OH*/CH* are sensitive to X_{NH3}, while NH*/CH* is less sensitive. The CH*/NH_2* ratio is an ideal marker of X_{NH3} in present laminar non-premixed NH_3-NH_4 flames, considering

that its chemiluminescence can be efficiently measured by economical visible-band photoelectric sensors.

(3) In the normal direction of a flame front, according to results from the Abel inverse transformation images, NH_2* is localized on the fuel side and CH* on the oxidant side, as well as OH* and NH* being localized in the intermedia zone of the flame front. An increase of X_{NH3} leads to greater flame thickness and shifts the peak value position of excited radicals further from the fuel side.

Author Contributions: Methodology, L.J.; Formal analysis, L.J.; Investigation, H.S. and J.Y.; Data curation, H.S. and Y.W.; Writing—original draft, H.S.; Writing—review & editing, L.J. All authors have read and agreed to the published version of the manuscript.

Funding: This work was supported by the Guangdong Basic and Applied Basic Research Foundation (No. 2022B1515120047).

Data Availability Statement: The original contributions presented in this study are included in the article. Further inquiries can be directed to the corresponding author.

Conflicts of Interest: The authors declare no conflicts of interest.

References

1. Zamfirescu, C.; Dincer, I. Using ammonia as a sustainable fuel. *J. Power Sources* **2008**, *185*, 459–465. [CrossRef]
2. Kumar, L.; Sleiti, A.K. Systematic review on ammonia as a sustainable fuel for combustion. *Renew. Sustain. Energy Rev.* **2024**, *202*, 114699. [CrossRef]
3. Kobayashi, H.; Hayakawa, A.; Somarathne, K.D.; Okafor, E.C. Science and technology of ammonia combustion. *Proc. Combust. Inst.* **2019**, *37*, 109–133. [CrossRef]
4. Docquierv, N.; Candel, S. Combustion control and sensors: A review. *Prog. Energy Combust. Sci.* **2002**, *28*, 107–150. [CrossRef]
5. Panoutsos, C.; Hardalupas, Y.; Taylor, A. Numerical evaluation of equivalence ratio measurement using OH* and CH* chemiluminescence in premixed and nonpremixed methane–air flames. *Combust. Flame* **2009**, *156*, 273–291. [CrossRef]
6. Guethe, F.; Guyot, D.; Singla, G.; Noiray, N.; Schuermans, B. Chemiluminescence as diagnostic tool in the development of gas turbines. *Appl. Phys. B* **2012**, *107*, 619–636. [CrossRef]
7. Pugh, D.; Runyon, J.; Bowen, P.; Giles, A.; Valeramedina, A.; Marsh, R.; Goktepe, B.; Hewlett, S. An investigation of ammonia primary flame combustor concepts for emissions reduction with OH*, NH_2* and NH* chemiluminescence at elevated conditions. *Proc. Combust. Inst.* **2021**, *38*, 6451–6459. [CrossRef]
8. Zhu, X.; Khateeb, A.A.; Roberts, W.L.; Guiberti, T.F. Chemiluminescence signature of premixed ammonia-methane-air flames. *Combust. Flame* **2021**, *231*, 111508. [CrossRef]
9. Weng, W.; Aldén, M.; Li, Z. Visible chemiluminescence of ammonia premixed flames and its application for flame diagnostics. *Proc. Combust. Inst.* **2023**, *39*, 4327–4334. [CrossRef]
10. Guiberti, T.F.; Shohdy, N.N.; Santiago, C.; Zhu, X.; Selle, L.; Lapeyre, C.J. Chemiluminescence- and machine learning-based monitoring of premixed ammonia-methane-air flames. *Appl. Energy Combust. Sci.* **2023**, *16*, 100212. [CrossRef]
11. Ku, J.W.; Choi, S.; Kim, H.K.; Lee, S.; Kwon, O.C. Extinction limits and structure of counterflow nonpremixed methane-ammonia/air flames. *Energy* **2018**, *165*, 314–325. [CrossRef]
12. Tu, Y.; Xu, S.; Liu, H. Combustion and emission characteristics of NH_3/CH_4/air in a model swirl combustor:Comparison between premixed and non-premixed modes. *Int. J. Hydrogen Energy* **2023**, *48*, 17311–17323. [CrossRef]
13. Elie, A.; Etienne, R. Intrinsic combustion instabilities in ammonia-hydrogen/methane non-premixed flames. *Proc. Combust. Inst.* **2024**, *40*, 105203. [CrossRef]
14. Jiang, L.; Gu, C.; Huo, J.; Yang, W. Improved two-color method for temperature measurement of soot flames. *J. Thermophys. Heat Transf.* **2022**, *36*, 431–439. [CrossRef]
15. Daun, K.J.; Thomson, K.A.; Liu, F.; Smallwood, G.J. Deconvolution of axisymmetric flame properties using Tikhonov regularization. *Appl. Opt.* **2006**, *45*, 4638–4646. [CrossRef]
16. Leipertz, A.; Obertacke, R.; Wintrich, F. Industrial combustion control using UV emission tomography. *Symp. (Int.) Combust.* **1996**, *26*, 2869–2875. [CrossRef]
17. Zhang, D.; Gao, Q.; Li, B.; Liu, J.; Li, Z. Ammonia measurements with femtosecond laser-induced plasma spectroscopy. *Appl. Opt.* **2019**, *58*, 1210–1214. [CrossRef]

18. Kopp, M.; Brower, M.; Mathieu, O.; Petersen, E.; Güthe, F. CO_2* chemiluminescence study at low and elevated pressures. *Appl. Phys. B* **2012**, *107*, 529–538. [CrossRef]
19. Samaniego, J.M.; Egolfopoulos, F.N.; Bowman, C.T. CO_2* Chemiluminescence in Premixed Flames. *Combust. Sci. Technol.* **1995**, *109*, 183–203. [CrossRef]
20. Han, X.; Wang, Z.; Costa, M.; Sun, Z.; He, Y.; Cen, K. Experimental and kinetic modeling study of laminar burning velocities of NH_3/air, NH_3/H_2/air, NH_3/CO/air and NH_3/CH_4/air premixed flames. *Combust. Flame* **2019**, *206*, 214–226. [CrossRef]
21. García-Armingol, T.; Ballester, J. Flame chemiluminescence in premixed combustion of hydrogen-enriched fuels. *Int. J. Hydrogen Energy* **2014**, *39*, 11299–11307. [CrossRef]
22. Issayev, G.; Zhu, X.; Capriolo, G.; Guiberti, T. Spatially resolved NH* and OH* profiles in ammonia-hydrogen-air counterflow diffusion flames. *Proc. Combust. Inst.* **2024**, *40*, 105427. [CrossRef]
23. Chen, D.; Li, J.; Li, X.; Guo, Y.; Huang, H.; Kobayashi, N. Experimental studies on the OH* chemiluminescence and structure characteristics in NH_3/H_2 and NH_3/cracked gas swirl flames. *Int. J. Hydrogen Energy* **2024**, *52*, 1370–1379. [CrossRef]
24. Zhang, H.; Han, X.; Jiang, J.; Li, X.; Gan, X.; Zhou, B. Numerical study of experimental feasible heat release rate markers for NH_3–H_2-air premixed flames. *Int. J. Hydrogen Energy* **2022**, *47*, 28165–28175. [CrossRef]
25. Zhu, X.; Guiberti, T.F.; Li, R.; Roberts, W.L. Numerical study of heat release rate markers in laminar premixed Ammonia-methane-air flames. *Fuel* **2022**, *318*, 123599. [CrossRef]
26. Konnov, A.A. An exploratory modelling study of chemiluminescence in ammonia-fuelled flames. Part 1. *Combust. Flame* **2023**, *253*, 112788. [CrossRef]
27. Kathrotia, T.; Fikri, M.; Bozkurt, M.; Hartmann, M.; Riedel, U.; Schulz, C. Study of the H+O+M reaction forming OH*: Kinetics of OH* chemiluminescence in hydrogen combustion systems. *Combust. Flame* **2010**, *157*, 1261–1273. [CrossRef]
28. Konnov, A.A. An exploratory modelling study of chemiluminescence in ammonia-fuelled flames. Part 2. *Combust. Flame* **2023**, *253*, 112789. [CrossRef]
29. Hayakawa, A.; Goto, T.; Mimoto, R.; Arakawa, Y.; Kudo, T.; Kobayashi, H. Laminar burning velocity and Markstein length of ammonia/air premixed flames at various pressures. *Fuel* **2015**, *159*, 98–106. [CrossRef]
30. Farber, M.; Darnell, A.J. Spectroscopic Examination of the NH_3–HNO_3 and NH_3–NO_2 Diffusion Flames. *J. Chem. Phys.* **1954**, *22*, 1261–1263. [CrossRef]
31. Mashruk, S.; Zhu, X.; Roberts, W.L.; Guiberti, T.F.; Valera-Medina, A. Chemiluminescent footprint of premixed ammonia-methane-air swirling flames. *Proc. Combust. Inst.* **2023**, *39*, 1415–1423. [CrossRef]

Disclaimer/Publisher's Note: The statements, opinions and data contained in all publications are solely those of the individual author(s) and contributor(s) and not of MDPI and/or the editor(s). MDPI and/or the editor(s) disclaim responsibility for any injury to people or property resulting from any ideas, methods, instructions or products referred to in the content.